Part III

Billiards

A large class of mechanical systems is called billiards in the chaos literature. The billiards considered here are 2-dimensional dynamical systems consisting of a point particle bouncing elastically off the billiard walls. The motion between collisions is either a free motion with constant velocity or an other simple motion for example a fall in a constant gravitational field.

We shall here present a general method to describe these systems with symbolic dynamics. We show on a number of examples that we can construct a well ordered symbol plane and a pruning front in this symbol plane. The method gives systematic approximate Markov partitions and approximate zeta functions that we expect to have better convergence than what can be obtained by expansions obtained by a simple numerical searches for periodic orbits. There are at present no other methods for describing the admissible orbits, except exhaustive numerical search for all periodic orbits up to a given length.

Some billiards, for example the 3-disk system can easily be identified with a Smale horseshoe for some parameter values, and a well-ordered symbol plane can be established. In other cases, like the stadium and the wedge billiard there is no direct correspondence to a simple horseshoe, but the idea of keeping the ordering by finding which symbols preserve or reverse the ordering still applies.

In the billiards we consider here there are no stable orbits. The bifurcations take place with the stable and the unstable manifolds crossing at a finite angle. The limiting orbits are singular orbits, analog to the orbits from the critical point of the tent map. Billiards are important as a test of the pruning front idea of Cvitanović et.al. [53], as the pruning front are here *exact* and not resting on conjectures, as is the case for the Hénon map and the smooth potentials we study in chapter 10.

Chapter 6

Symbolic dynamics of billiards

Our goal is to find a way to describe the orbits in the billiard systems by applying symbolic dynamics. This will be different than the methods applied by Sinai and others which proof for some billiards the existence of a countable Markov partition. As our first step we will define a covering symbolic description of the system, which is exact in one limit of parameters, or symbols which always give a unique description of orbits existing but which also describe orbits not existing in the system. In the case of billiards that give a complete Smale horseshoe non-wandering set, the definition of symbols is straightforward. In other systems finding a good symbolic description may be more difficult, but we outline a general method for approaching this problem.

The second important step, necessary for determining the symbolic strings corresponding to admissible orbits is to determine a symbolic representation of orbits which has an orientation topologically faithful to the orientation of the foliation of stable and unstable manifolds in the phase space. This is necessary because the mechanism giving forbidden orbits reflects this ordering in the phase space. This is the case for all examples given here and we conjecture that this is, if not always true, at least typical for most systems.

There is unfortunately no general theory for construction of symbolic dynamics for an arbitrary dynamical system. For each new system one has to *think* before defining the symbols. However, for simple billiard systems it seems that giving one symbol for each bounce off the different dispersive walls, and two symbols for focusing walls; one for clockwise and one for counterclockwise bounces suffices. Fictitious straight walls introduced to reduce the dynamics to a fundamental domain can also be given one symbol each. If there are other forces in the system, like gravity or rotation, other definitions of the symbols may be required.

A correctly ordered symbol alphabet is obtained from the first alphabet by

investigating how the symbolic description of the orbit changes when we change one of the phase space variables. If the non-wandering set in some limit of parameters is a complete Smale horseshoe then we define the new symbols from one of the alphabets introduced in chapter 3. at each level of the Cantor set such symbols increase as we scan across the vertical strips and the horizontal strips. If there is no limit in which the billiard is a complete horseshoe, we define well ordered symbols by using the same method of ordering the vertical and horizontal strips in phase space. In general the strips are overlapping and not complete, and strips corresponding to some symbol string may not exist. We first assume the strips are complete, then construct the well ordered symbols and finally remove from the symbol plane the parts of the strips that do not exist in phase space. Examples of such systems are the stadium (section 6.5) and the wedge billiard (section 6.4).

6.1 3-disk

The simplest example of a billiard is the 3 disk system. The 3 disk system consists a point particle moving freely on a 2-dimensional plane and bouncing elastically off the walls of 3 disks placed in the plane. We will mostly work with the symmetric system where the 3 disks have the same radius, and the same distance between any two disks. In this system we set the radius to be 1 and choose the parameter r to be the distance between the centers of the disks. This system is studied by Eckhardt and Cvitanović [66, 48], Gaspard and Rice [83, 82] and others.

We choose the bounce of the particle off one disk to be our Poincaré map. The 1-dimensional position along the edge of the disk x, and the angle ϕ, between the normal vector of the wall and the direction of the outgoing velocity are variables sufficient to uniquely specify an orbit. In the symmetric 3 disks system the three disks yield the same Poincaré map. For some configurations of the 3 disks system this two dimensional Poincaré map gives a once folding complete horseshoe with two vertical and two horizontal strips ordered as in figure 3.13. In the symmetric system this configuration is obtained by choosing the distance between the disks sufficiently large.

The two horseshoe strips are constructed as follows: we choose to observe the particle when it bounces off the disk that we denote no. 1. The other disks are enumerated counterclockwise as no. 2 and no. 3. If the particle bounces out from point x then there are two intervals of the angle ϕ which give a new bounce in one of the other two disks. In figure 6.1 we draw the outgoing angles. Doing this for all x-values gives two strips sketched in figure 6.2 a). This is the first generation in

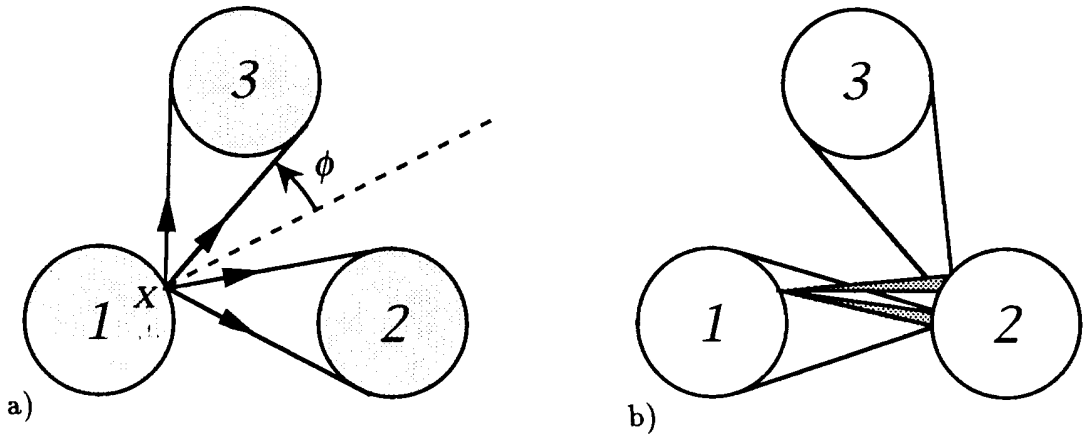

Figure 6.1: a) The 3 disk system and the phase space variables. b) Orbits of different angles bouncing into the next disk.

the construction of the forward Cantor set which corresponds to the vertical strips in the horseshoe map in figure 3.11. We use Smale's horseshoe notation and call these two strips $g(Q) \cap Q$. The strips are limited to the region

$$-\pi/2 \leq x \leq 2\pi/3, \quad -\pi/2 \leq \phi \leq \pi/2 \tag{6.1}$$

An angle $|\phi| > \pi/2$ would correspond to a particle penetrating the disk. If x is less than $-\pi/2$ or larger than $2\pi/3$ one can not reach either of the other disks.

The two strips are given symbolic description by recording the labels of the two disks that the particle has bounced off. This gives the two symbolic strings

$$\{12, 13\}. \tag{6.2}$$

In figure 6.2 a) the lower strip is 12 and the upper strip is 13.

The next generation in this Cantor set of strips, $g^{(2)}(Q) \cap Q$, is obtained by finding all points in (x, ϕ) for which the outgoing particle reaches at least two disks. In figure 6.1 b) we have drawn the orbits from disk 1 that first bounce off disk 2, and then reach either disk 1 or 3. This are two intervals of angles strictly inside the interval giving one bounce off disk 2. In the phase space this gives four strips strictly inside the two first strips, figure 6.2 b), with the symbolic descriptions

$$\{121, 123, 132, 131\} \tag{6.3}$$

ordered from the lowermost strip to the uppermost strip. The third level of the Cantor set, figure 6.2 c), gives eight strips and their symbolic description from the lowermost to the uppermost is

$$\{1212, 1213, 1231, 1232, 1323, 1321, 1312, 1313\} \tag{6.4}$$

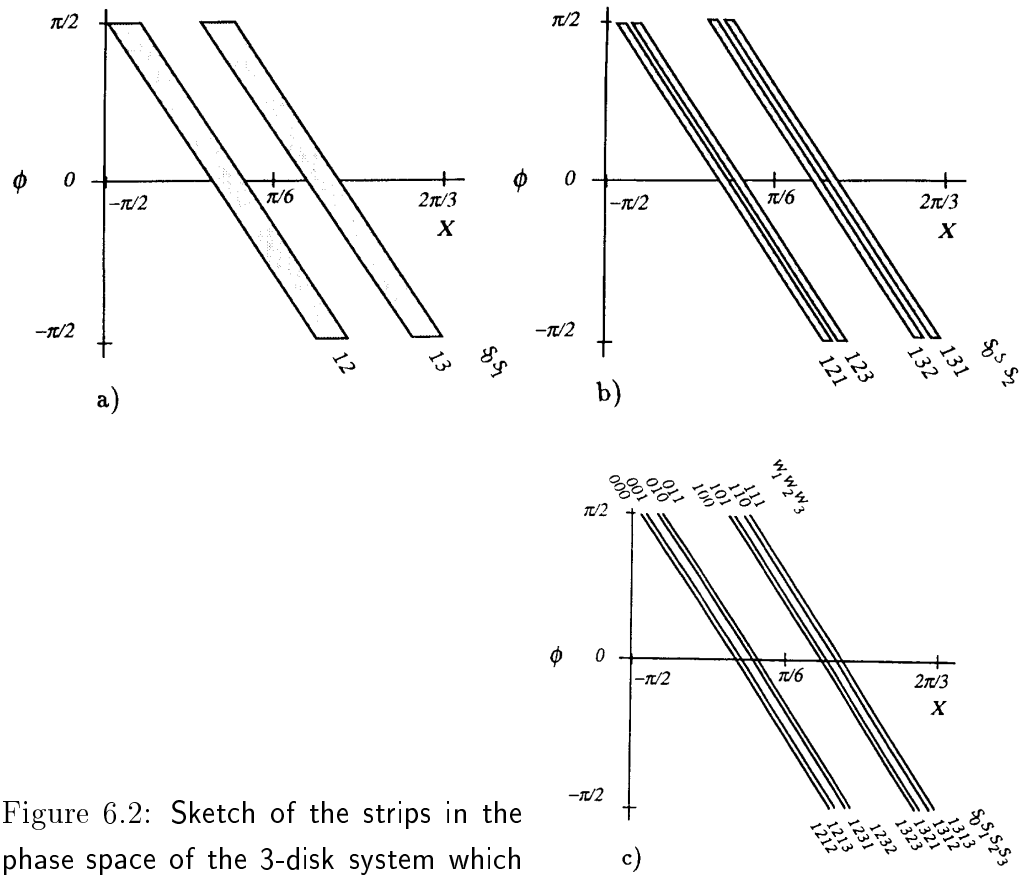

Figure 6.2: Sketch of the strips in the phase space of the 3-disk system which correspond to a point bouncing in the system at least a) once, b) twice, c) three times.

In this way we construct the forward Cantor set of lines as the union of all orbits that continue to bounce between the disks forever. Each line in the Cantor set has a unique label

$$s_0 s_1 s_2 s_3 \ldots \tag{6.5}$$

where $s_i \in \{1, 2, 3\}$. Since this is a binary Cantor set, a three letter alphabet is larger than necessary. A two letter alphabet description can be obtained by choosing the letter $v_i = 0$ if the bounce is counterclockwise, that is if $s_{i-1}s_i = 12$ or 23 or 31, and choosing the letter $v_i = 1$ if the bounce is clockwise $s_{i-1}s_i = 13$ or 21 or 32. We can state this as the algorithm

$$\begin{aligned} & v'_i = s_i - s_{i-1} \\ & \text{if } v'_t < 0 \text{ then } \; v_t = v'_t + 2 \\ & \text{else } \; v_t = v'_t - 1 \end{aligned} \tag{6.6}$$

In the case of a symmetric system one does not need to remember the starting disk. This two letter alphabet $v_i \in \{0, 1\}$ is then the alphabet corresponding to the alphabet used in the Smale horseshoe. A time iteration of this orbit corresponds to a simple shift in the symbol sequence.

Because of the dispersive mirror reflection at each disk both strips change the orientation both forward and backward in time as in figures 3.13 and 3.13. We will below discuss the different change in orientation for bounces off dispersing or focusing walls. We then obtain well ordered symbols by the algorithm (3.9)

$$\begin{aligned} w_t &= \begin{cases} v_t & \text{if } t \text{ odd } > 0 \\ 1 - v_t & \text{if } t \text{ even } > 0 \end{cases} \\ w_t &= \begin{cases} v_t & \text{if } t \text{ even } \leq 0 \\ 1 - v_t & \text{if } t \text{ odd } < 0 \end{cases} \end{aligned} \tag{6.7}$$

The strips in figure 6.2 c) are also labeled by the symbol strings $w_1 w_2 w_3$ and we find that from the lowermost to the uppermost they are ordered as

$$\{000, 001, 010, 011, 100, 101, 110, 111\} \tag{6.8}$$

A symbolic value

$$\gamma = 0.w_1 w_2 w_3 \ldots = \sum_{t=1}^{\infty} \frac{w_t}{2^t} \tag{6.9}$$

then increases along any curve that monotonously crosses the lines in the Cantor set, exactly as a well ordered forward symbolic value should do.

The backward iteration is found by finding the orbits that arrived at the point (x, ϕ). Some of these orbits have been bouncing off one of the other two disks before reaching the point (x, ϕ), and this gives the two strips corresponding to the backward iteration of the Smale horseshoe $g^{(-1)}(Q) \cap Q$. These are the vertical strips in the horseshoe picture. Since we know that the incoming angle is the negative of the outgoing angle (time reversal invariance) we obtain the strips $g^{(-1)}(Q) \cap Q$ by reflecting the strips $g(Q) \cap Q$ around the x-axis. These strips and the four rectangles $g(Q) \cap g^{(-1)}(Q)$ are sketched in figure 6.3 a).

The two backward strips $g^{(-1)}(Q) \cap Q$ have the symbolic description $s_{-1} s_0 \in \{21, 31\}$. In the same way as for the future symbols we define v_i as the symbol giving either a clockwise or an anticlockwise bounce. The well ordered symbol w_i is also given by (3.8) and we define the symbolic value for the past to be

$$\delta = 0.w_0 w_{-1} w_{-2} \ldots = \sum_{t=1}^{\infty} \frac{w_{1-t}}{2^t} \tag{6.10}$$

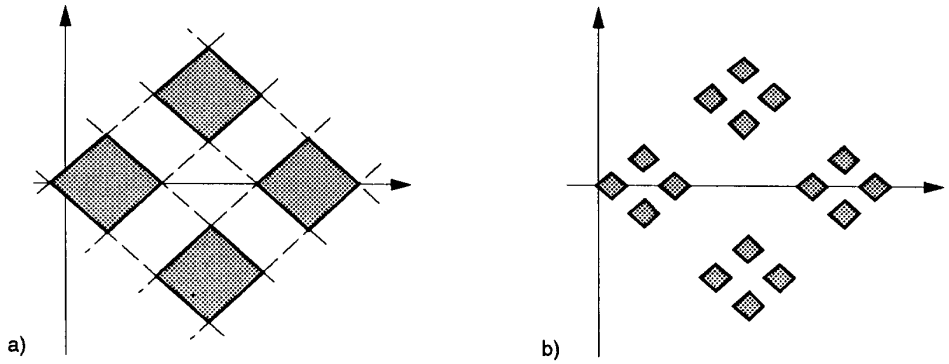

Figure 6.3: Sketch of the points in the phase space of the 3 disk system which correspond to an orbit bouncing both in the future and past at least a) once, b) twice.

Figure 6.4: The fundamental domain of the 3 disk system.

This value δ gives the correct ordering of the backward strips and the symbolic value plane (γ, δ) represents all points in the non-wandering set ordered the same way as in the phase space. In figure 6.3 b) the values for the 16 rectangles of $g^{(2)}(Q) \cap g^{(-2)}(Q)$ are drawn and we find that the γ-axis is a curve going down left in (x, ϕ) and the δ-axis is a curve going up left in (x, ϕ).

If the 3 disk system is symmetric then the (γ, δ) plane is the same for all three disks. Time symmetry implies that (γ, δ) is equal (δ, γ), and the phase space (x, ϕ) symmetry around the line $x = \pi/6$ implies that (δ, γ) is equal $(1 - \gamma, 1 - \delta)$. One may study the dynamics in the fundamental domain, a 6-th of the original system, see figure 6.4.

If the 3 disk system is not symmetric, then the pruning may look different in the symbolic planes of the different orbits, and is not necessarily symmetric.

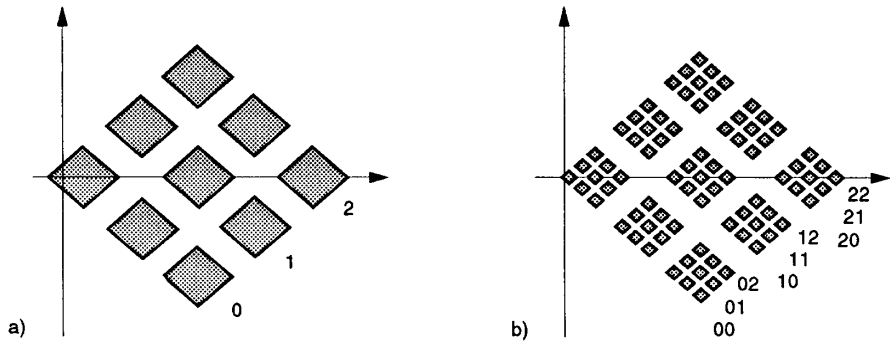

Figure 6.5: Sketch of the points in the phase space of the 4 disk system giving an orbit bouncing in the future and past at lest a) once, b) twice.

6.2 4-disk

The system with a particle bouncing between 4 disks gives a Cantor set in a way very similar to the 3 disk system, but with 3 strips in each generation of the Cantor set, like the three folding Smale horseshoe. If we have a symmetric four disk system with sufficiently separated disks, then the non-wandering set is the the same, as in the complete three folding Smale horseshoe. The orientation changes for all three folds in the horseshoe.

We enumerate the disks anticlockwise, $s_i \in \{1,2,3,4\}$, and obtain the well ordered symbols $w_i \in \{0,1,2\}$ by the algorithm

$$\begin{aligned} v_t &= s_t - s_{t-1} \\ &\text{if } v_t < 1 \text{ then } v_t = v_t + 4 \\ w_t &= \begin{cases} v_t - 1 & \text{if } t \text{ odd} \\ 3 - v_t & \text{if } t \text{ even} \end{cases} \end{aligned} \tag{6.11}$$

The symbolic values for the future and past are base 3 numbers given as

$$\gamma = 0.w_1 w_2 w_3 \ldots = \sum_{t=1}^{\infty} \frac{w_t}{3^t} \tag{6.12}$$

$$\delta = 0.w_0 w_{-1} w_{-2} \ldots = \sum_{t=1}^{\infty} \frac{w_{1-t}}{3^t} \tag{6.13}$$

A sketch of the first generation of the Cantor set in the phase space with the symbols w_i is drawn in figure 6.5. For the symmetric 4-disk system, another convenient choice of a symbolic alphabet are the three discrete group operations C_2, σ_x and σ_y [49]. The relationship between the group operations denoted $g_i \in \{C_2, \sigma_x, \sigma_y\}$ and

the well ordered symbols $w_i \in \{0,1,2\}$ is given by the algorithm

$$\begin{aligned} v_i &= \begin{cases} 0 & \text{if} \quad g_i = \sigma_x \\ 1 & \text{if} \quad g_i = C_2 \\ 2 & \text{if} \quad g_i = \sigma_y \end{cases} \\ r_i &= \begin{cases} r_i + 1 & \text{if} \quad g_i = C_2 \\ r_i & \text{else} \end{cases} \\ w_i &= \begin{cases} v_i & \text{if} \quad r_i \text{ odd} \\ 2 - v_i & \text{if} \quad r_i \text{ even} \end{cases} \end{aligned} \tag{6.14}$$

The symbols g_i can be obtained from w_i by

$$\begin{aligned} g'_i &= \begin{cases} \sigma_x & \text{if} \quad w_i = 0 \\ C_2 & \text{if} \quad w_i = 1 \\ \sigma_y & \text{if} \quad w_i = 2 \end{cases} \\ r_i &= \begin{cases} r_i + 1 & \text{if} \quad w_i = 1 \\ r_i & \text{else} \end{cases} \\ g_i &= \begin{cases} C_2 & \text{if} \quad g'_i = C_2 \\ \sigma_x & \text{if} \quad g'_i = \sigma_x \text{ and } r_t \text{ is even} \\ \sigma_x & \text{if} \quad g'_i = \sigma_y \text{ and } r_t \text{ is odd} \\ \sigma_y & \text{if} \quad g'_i = \sigma_x \text{ and } r_t \text{ is odd} \\ \sigma_y & \text{if} \quad g'_i = \sigma_y \text{ and } r_t \text{ is even} \end{cases} \end{aligned} \tag{6.15}$$

6.3 N-disk systems

Assume the system consists of N disks. If the disks are well separated, the non-wandering set is a Cantor set of the Smale horseshoe type, with one symbol for bouncing into each of the other disks. This symbolic description can be turned into a well ordered alphabet as we have done it for the 3 and 4 disk systems, but the algorithm translating from the alphabet s_t of enumerated disks to the well ordered alphabet w_t can become rather complicated. We show this algorithm for a few N-disk systems with special symmetry.

6.3.1 Symbolic dynamics for N disks on a circle

Let N equal disks have the center of each disk on a large circle, and let r, the distance between centers of neighbor disks on the large circle, be large. Then Λ_1^+ consists of $(N-1)$ strips in the phase space. The well ordered symbols $w_t \in \{0,1,2\ldots,(N-2)\}$

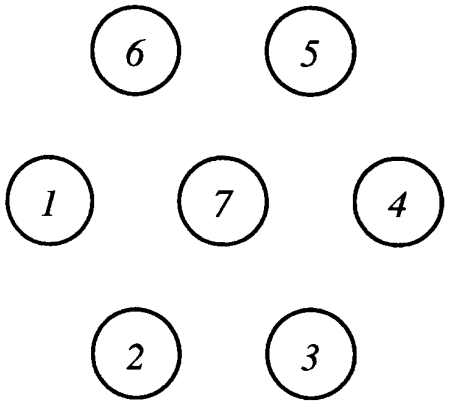

Figure 6.6: The configuration space of the 6+1 disk system.

are constructed from the anticlockwise enumeration of the disks $s_t \in \{1, 2, \ldots, N\}$ using the algorithm

$$\begin{aligned} v &= s_t - s_{t-1} \\ &\text{if} \quad v_t < 1 \quad \text{then} \quad v_t = v_t + N \\ w_t &= \begin{cases} v_t - 1 & \text{if} \quad t \text{ odd} \\ N - v_t - 1 & \text{if} \quad t \text{ even} \end{cases} \end{aligned} \tag{6.16}$$

When $N = 3$ this is the same algorithm as (6.7), and for $N = 4$ this is the algorithm (6.11). From w_t we construct base $(N-1)$ symbolic coordinates $\gamma = 0.w_1 w_2 w_3 \ldots = \sum_{t=1}^{\infty} w_t/(N-1)^t$ and $\delta = 0.w_0 w_{-1} w_{-2} \ldots = \sum_{t=1}^{\infty} w_{1-t}/(N-1)^t$ where $0 \leq \gamma, \delta \leq 1$.

6.3.2 N disks with a center disk

Let the billiard be a configuration of N disks on a large circle as in the billiard above and in addition one disk in the center of this large circle. The radius of each disks is 1, and the distance between two neighbor disks is r. The disks on the circle is enumerated anticlockwise from 1 to N ,and a bounce off the disk in the center is given the symbol $(N + 1)$. Figure 6.6 shows this configuration with $N = 6$. If the number of disks on the large circle is even, then, because of the disk in the center, a point particle can not bounce between two disks opposite to each other on the large circle. From the $(N + 1)$ symbols of the disks, we get $(N - 1)$ well ordered symbols, and Λ_1^+ $(= g(Q) \cap Q)$ consists of $(N - 1)$ strips in the phase space. With N (even) disks on the large circle and the center disk with symbol $(N + 1)$, the

algorithm defining the well ordered symbols $w_t \in \{0, 1, 2 \ldots, (N-2)\}$ is

$$
\begin{array}{lll}
\text{if} & s_t = (N+1) & \text{then} \quad w_t = (N-2)/2 \\
\text{else if} & s_{t-1} \neq (N+1) & \text{then} \\
& v_t = s_t - s_{t-1} & \\
& \text{if} \quad v_t < 1 & \text{then} \quad v_t = v_t + N \\
& w_t \quad = & \begin{cases} v_t - 1 & \text{if} \quad t \text{ odd} \\ N - v_t - 1 & \text{if} \quad t \text{ even} \end{cases} \\
\text{else if} & s_{t-1} = (N+1) & \text{then} \\
& v_t = s_t - s_{t-2} & \\
& \text{if} \quad v_t < -(N-2)/2 & \text{then} \quad v_t = v_t + N \\
& \text{if} \quad v_t > (N-2)/2 & \text{then} \quad v_t = v_t - N \\
& w_t \quad = & \begin{cases} (N-2)/2 + v_t & \text{if} \quad t \text{ odd} \\ (N-2)/2 - v_t & \text{if} \quad t \text{ even} \end{cases}
\end{array}
\tag{6.17}
$$

$$
\gamma \quad = \quad 0.w_1 w_2 w_3 \ldots = \sum_{t=1}^{\infty} \frac{w_t}{(N-1)^t} \tag{6.18}
$$

$$
\delta \quad = \quad 0.w_0 w_{-1} w_{-2} \ldots = \sum_{t=1}^{\infty} \frac{w_{1-t}}{(N-1)^t} \tag{6.19}
$$

The configuration with $N = 6$ can be looked at as a first step toward a description of the Lorentz gas [137, 181], a triangular lattice with a hard disk in each lattice point and a point particle scattering in the lattice.

If the number of disks N on the large circle is odd and the disks are sufficiently separated, a point particle can reach all other disks after bouncing off one disk. The algorithm giving the symbols $w_t \in \{0, 1, 2 \ldots, (N-1)\}$ is

$$
\begin{array}{lll}
\text{if} & s_t = (N+1) & \text{then} \quad w_t = (N-1)/2 \\
\text{else if} & s_{t-1} \neq (N+1) & \text{then} \\
& v_t = s_t - s_{t-1} & \\
& \text{if} \quad v_t < 1 & \text{then} \quad v_t = v_t + N \\
& w_t \quad = & \begin{cases} v_t - 1 & \text{if} \quad t \text{ odd} \\ N - v_t - 1 & \text{if} \quad t \text{ even} \end{cases} \\
& \text{if} \quad w_t > (N-1)/2 & \text{then} \quad w_t = w_t + 1 \\
\text{else if} & s_{t-1} = (N+1) & \text{then} \\
& v_t = s_t - s_{t-2} & \\
& \text{if} \quad v_t < -(N-1)/2 & \text{then} \quad v_t = v_t + N \\
& \text{if} \quad v_t > (N-1)/2 & \text{then} \quad v_t = v_t - N \\
& w_t \quad = & \begin{cases} (N-1)/2 + v_t & \text{if} \quad t \text{ odd} \\ (N-1)/2 - v_t & \text{if} \quad t \text{ even} \end{cases}
\end{array}
\tag{6.20}
$$

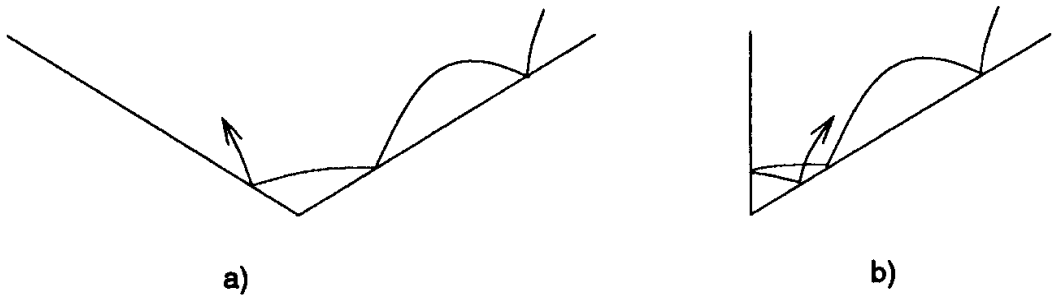

Figure 6.7: The wedge billiard. a) The whole domain. b) The fundamental domain.

6.4 Wedge billiard, or Two Bouncing Balls

The next example is another type of a billiard system, which has two mechanical realizations both described by the same mathematics. We first describe the physics of the two problems and how they are related to each other.

6.4.1 Wedge billiard

One realization is given by a point particle with a mass m moving in a plane with constant gravitation, and bouncing off two symmetrically tilted planes, figure 6.7 a). This system was introduced and studied numerically by Lehtihet and Miller [131]. The system can be reduced to the the fundamental domain billiard in figure 6.7 b) with a vertical wall replacing one of the tilted walls. Two orbits which are symmetric to each other with respect to the y-axis in the full domain are mapped into the same orbit in the fundamental domain, and correspondingly a single orbit in the fundamental domain can correspond to two full space orbits. A periodic orbits in the fundamental domain is mapped into only one orbit in the full domain if this orbit is symmetric with respect to the y-axis in the full domain.

The Hamiltonian for this system is

$$H = \frac{1}{2}\left(p_x^2 + p_y^2\right) + y, \quad x > 0, \;\; y > x\cot\phi. \tag{6.21}$$

At the collision with the tilted wall the perpendicular component of the momentum switches direction.

Lehtihet and Miller[131] have shown that this flow can be turned into a map as follows: Let $\vec{e}_r$ be the unity vector pointing from the tip of the wedge to the position of the ball, and $\vec{e}_\phi$ be the unity tangent vector orthogonal to $\vec{e}_r$. Let $\vec{v}$ be

the velocity of the ball. The map T is given by (x and y are respectively the radial and the tangential components of the velocity vector):

$$\begin{array}{rcl} & \text{if} & (x_t - 2y_t)^2 \cos^2\theta + y_t^2 \sin^2\theta < 1 \\ T_0 \;:\; \left\{ \begin{array}{rcl} x_{t+1} &=& x_t - 2y_t \\ y_{t+1} &=& y_t \end{array} \right. & & \\ & \text{else} & \\ T_1 \;:\; \left\{ \begin{array}{rcl} x_{t+1} &=& y_t - x_t - y_{t+1} \\ y_{t+1} &=& \sqrt{2 + 2\xi(y_t - x_t)^2 - y_t^2} \end{array} \right. , & & \xi = \frac{1-\tan^2\theta}{(1+\tan^2\theta)^2} \,. \end{array} \tag{6.22}$$

The map T_0 corresponds to two consecutive bounces off the inclined plane, while map T_1 describes the particle bouncing from the inclined plane to the vertical wall and then back again to the inclined plane. The time reversal amounts to reversing the velocity component parallel to the plane of reflection, $x \to -x$:

$$T_i^{-1} = \tau^{-1} T_i \tau \qquad \tau = \begin{bmatrix} -1 & 0 \\ 0 & 1 \end{bmatrix} , \tag{6.23}$$

The phase space is manifestly symmetric under reflection across the y-axis.

6.4.2 Two Bouncing Balls

A second problem that gives rise to the same dynamical system is the system of two balls moving along a vertical line in constant gravitational field. The upper ball, no. 2, has mass m_2 and bounces elastically off the ball below. The ball underneath, no. 1, with mass m_1, bounces off the floor and off the ball above. Figure 6.8 a) shows the the system, and motion in time is sketched in figure 6.8 b).

The Hamiltonian for the motion between the bounces is

$$H = \frac{p_1^2}{2m_1} + \frac{p_2^2}{2m_2} + m_1 q_1 + m_2 q_2 \tag{6.24}$$

When ball no. 1 bounces elastically off the floor we have

$$v_1 \to -v_1 \tag{6.25}$$

and at an elastic bounce between ball no. 1 and ball no. 2

$$\begin{array}{rcl} v_1 &\to& \gamma v_1 + (1-\gamma) v_2 \\ v_2 &\to& (1+\gamma) v_1 - \gamma v_2 \end{array} \tag{6.26}$$

where $\gamma = (m_1 - m_2)/(m_1 + m_2)$.

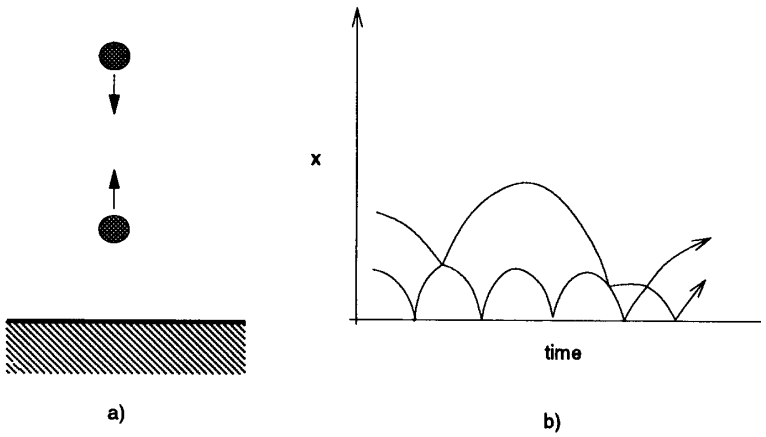

Figure 6.8: a) The two bouncing balls system in one dimension. b) The position of the balls as a function of time.

It was showed by Wojtkowsky [200] that this system has nonzero Lyapunov exponents for almost every starting point. He also showed that the linear change of variables

$$\begin{aligned} x_1 &= \sqrt{m_1 m_2}(q_1 - q_2) \\ x_2 &= m_1 q_1 + m_2 q_2 \\ p_{x_1} &= \sqrt{\frac{m_2}{m_1}} p_1 - \sqrt{\frac{m_1}{m_2}} p_2 \\ p_{x_2} &= p_1 + p_2 \end{aligned}$$

with masses normalized to $m_1 + m_2 = 1$, yields the Hamiltonian

$$H = \frac{1}{2}(p_{x_1} + p_{x_1}) + x_2 \tag{6.27}$$

in the configuration space

$$\begin{aligned} x_1 &\leq 0 \\ x_2 &\geq \frac{x_1}{\tan\theta} = \frac{m_2}{m_1} x_1 \end{aligned}$$

which is identical to the wedge billiard (6.21) in the fundamental domain.

This problem was first studied by Wojtkowski [200], and he also studied a generalizations of this problem to a problem with n bouncing balls in one dimension. Chernov [35] showed how Wojtkowski's proof of the local instability can be turned into a proof that this is an ergodic system for $m_1 > m_2$. A Galilei version of this problem can be done as a simple experimental demonstration of chaotic vs. integrable motion. An air pressure rail which exists in all physics teaching labs may be tilted a few degrees and with two wagons of different mass, stable and chaotic motion may be demonstrated.

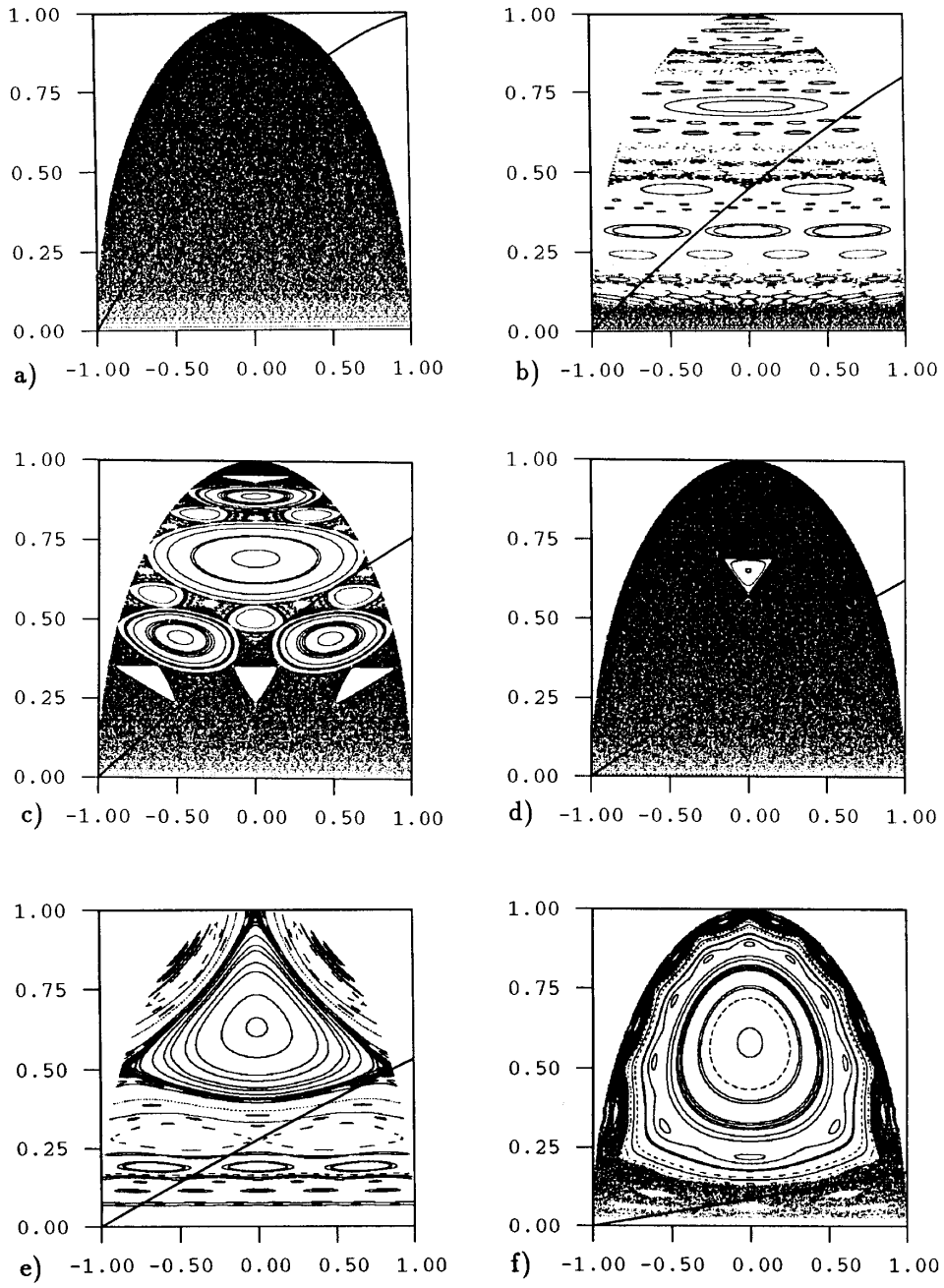

Figure 6.9: Different orbits in the wedge billiard. a) $\theta = 60°$ b) $\theta = 44.8°$ c) $\theta = 43°$ d) $\theta = 35°$ e) $\theta = 30°$ f) $\theta = 10°$

6.4.3 Numerical simulations

Simple numerical explorations revel a first picture of the dynamics of the system. We use the map (6.22) for numerical work. A few numerically obtained trajectories are shown in figure 6.9 for different values of the parameter θ. Lehtihet and Miller [131] have observed that for $\xi > 0$ there exist stable periodic orbits surrounded by KAM torii, and these bifurcate in a complicated way as the parameter changes. In the two ball system $\theta < 45$ corresponds to the upper ball has a larger mass $m_2 > m_1$.

Close to $\theta = 45^\circ$ these stable orbits organize into a Farey-tree like structure visible in figure 6.9 b). We explain below why this happens, and how it is expressed in symbolic dynamics as a tree construction of the admissible symbols.

In the limit of $\theta = 0^\circ$ the fixed point and the KAM tory around it dominates the whole phase space; in the limit of a very narrow wedge there exists a stable orbit of period 2 bouncing back and forth between the two walls. The other orbits are bouncing back and forth between the two walls and rotate around the short periodic orbit in the phase space. In the two ball picture this periodic orbit corresponds to the upper ball bouncing once off the ball below between each time this ball bounces off the floor.

The "wide" wedge billiard has an angle θ between 45° and 90°, which in the two ball system corresponds to the lower ball has a larger mass, $m_1 > m_2$. In figure 6.9 a) the parameter $\theta = 60^\circ$ and there are no stable islands anywhere in the phase space. Changing the parameter results in no visible difference when plotting a chaotic orbit in the phase space. The orbit does change, but the the Poincaré map only shows uniform ergodic distribution of trajectory points. Wojtkowski [200] showed for the two ball system, that for $m_1 > m_2$ almost all points have one positive Liapunov exponent, and Chernov [35] used this to prove the ergodicity of the system for these parameter values. He actually showed this for a more general system with not necessarily constant gravitation $V(q) = gq$ but with a force directed downward $V'(q) > 0$ not increasing with the height, $V''(q) \leq 0$.

The proof ensures that for $m_1 > m_2$ the stable and unstable manifolds are never parallel. A picture of the manifolds is obtained by iterating a short line segment along the unstable eigenvector of the fixed point $\overline{1}$. In figure 6.10 a line of length 0.001 starting at the fixed point is drawn, together with a number of iterations of the line. The same curves reflected across the y–axis trace out the stable manifold of the fixed point. As expected, the unstable and stable manifolds are nowhere parallel. However, in the limit $\theta \to 45^{\circ +}$ the stable and unstable manifolds become horizontal and tangent to each other, as expected, since for $\theta = 45^\circ$ the system is integrable, and all orbits are marginally stable.

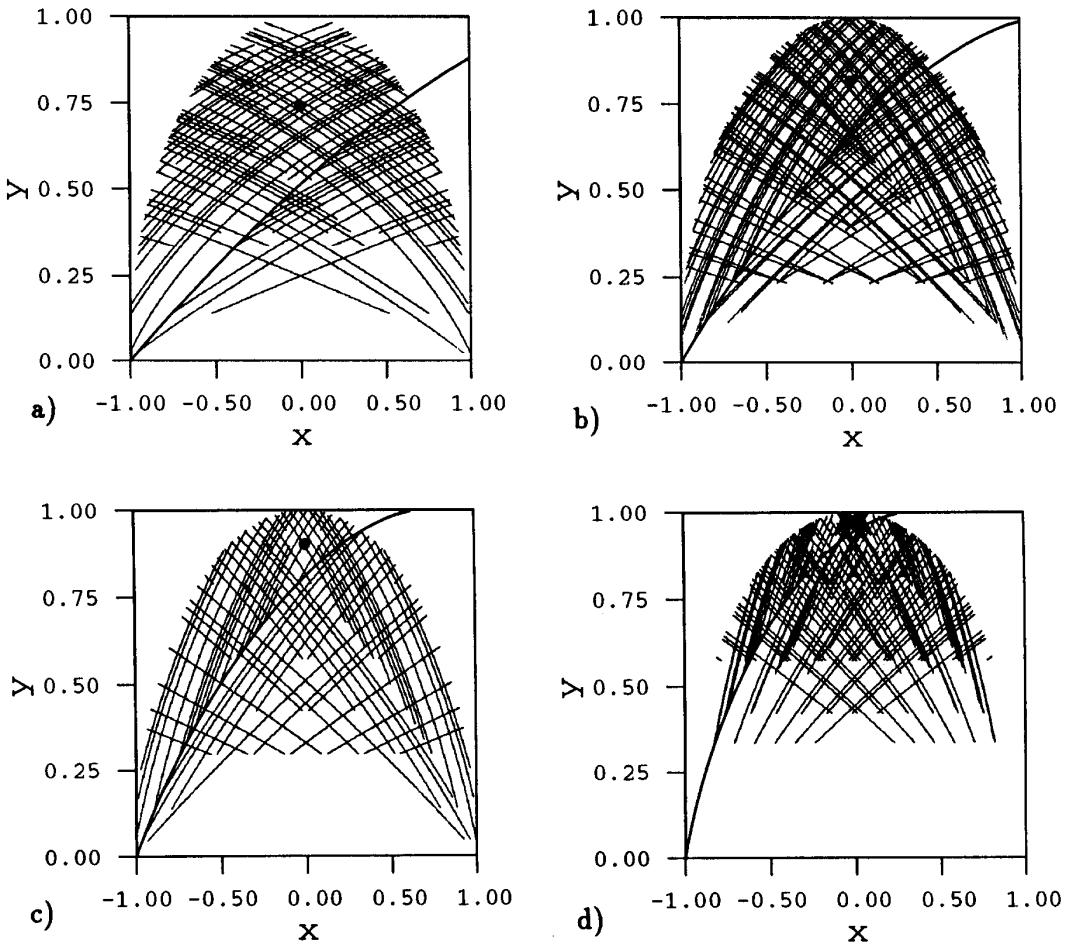

Figure 6.10: The stable and the unstable manifolds of the fixed point in the wedge billiard. a) $\theta = 50^\circ$ b) $\theta = 60^\circ$ c) $\theta = 70^\circ$ d) $\theta = 80^\circ$

6.4.4 Symbolic dynamics

The discontinuity in the map (6.22) suggests a natural way to define symbolic dynamics. Szeredi and Goodings [188, 189] denote a bounce of the ball from the tilted wall directly back to the tilted wall by the symbol T. The bounce from the tilted wall into the vertical wall and then back to the tilted wall they denote by V. We prefer to use 0 for their symbol T, and 1 for their symbol V. Using the map (6.22), we assign symbol 0 when the iteration is obtained by using map T_0, and symbol 1 when the iteration is according to map T_1. Szeredi and Goodings have tested this symbolic dynamics numerically and found that for the completely chaotic wedge billiard $45^\circ < \theta < 90^\circ$ this symbolic alphabet assigns a unique symbol string to each physically realized periodic orbit. They also found a lot of pruning, i.e. that many symbol strings did correspond to admissible orbits.

In the two ball system the same symbolic dynamics is obtained by assigning symbol 0 to be a bounce of ball no. 1 off the floor and then back to the floor without hitting the ball no. 2. The symbol 1 is assigned to the case where ball no. 1 bounces off the floor, bounces into ball no. 2, and then returns back to the floor. As long as $m_2 < m_1$, the two balls cannot collide more than once between two consecutive bounces off the floor.

The well ordered symbols for the map are determined by how the orientation changes under the maps T_0 and T_1. There is no limit of parameter values where the map is a complete horseshoe; instead we study the foliation of its stable and unstable manifolds. The map T_0 corresponds to a simple linear shear, with change in orientation. The map T_1 reverses the orientation in both the stable and the unstable directions. The fixed point $\overline{1}$ has two negative eigenvalues for all parameter values $m_1 > m_2$. The manifolds in figure 6.10 in the part of the phase space on which T_1 acts are reversed after one iteration.

A map with manifolds that have the same orientation under T_0 but where both manifolds are reversed under T_1 gives the same ordering of symbols as the once folding horseshoe without any reflection. The well ordered symbols are then obtained by the algorithms (1.18) and (3.5).

We will show below that there is always pruning in this system, so we cannot draw a complete cantor set for any parameter values.

6.5 Stadium Billiard

One of the best known challenges in nonlinear dynamics is the problem of the description of the Bunimovich stadium billiard [32]. The stadium and a segment

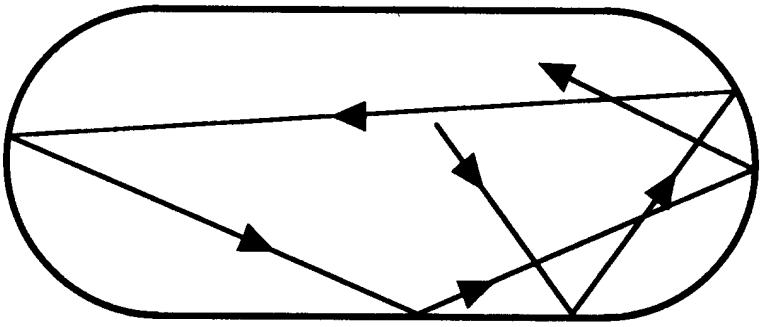

Figure 6.11: The stadium billiard and an orbit in this billiard.

of a typical orbit are drawn in figure 6.11. The system is a point particle moving freely inside and bouncing off the walls that consist of two semi-circles connected by two straight lines. We set the radius of the two semi-circles equal to 1 without any loss of generality. The length of the straight lines is the only parameter in the system, and we set it to $2a$. Bunimovich [32] proved that this system has a positive Liapunov exponent almost everywhere and that it is ergodic. There is a line of marginally stable cycles, orbits bouncing up and down between the two straight lines, while all other orbits are unstable.

The symbolic dynamics of the stadium is more complicated than in the systems studied above. The use of both straight walls and focusing walls as the border gives a more complicated algorithm for the well ordered symbols. Also, as in the wedge billiard, we cannot find a complete Smale horseshoe at any parameter values. But we show here that in the limit of infinity long straight walls there exist a Markov partition with a good choice of symbols.

The most interesting work on the symbolic dynamics of the stadium done so far is the article by Biham and Kvale [25]. They introduce a symbolic dynamics that we shall mostly follow here, and apply this finding numerically periodic orbits. They also discuss pruning of orbits and show how one may find a periodic orbit for each symbol string and check whether it is pruned The new results presented here are: implementation of the parameter independent (or "geometrical" [25]) pruning roles as a transition matrix, the topological entropy determined exactly in the $a \to \infty$ limit, and the description of parameter dependent (or "dynamical" [25]) pruning rules by a pruning front.

6.5.1 Phase space

A natural Poincaré map for the stadium is θ, the position of a bounce off the wall and ϕ, the outgoing angle of the particle. Since the system is ergodic a long chaotic orbit should visit arbitrarily close to all points in the phase space. Even so there are structures in the phase space that cannot be seen in a plot of the Poincaré map of one chaotic orbit. The structure of stable and unstable manifolds can be illustrated by iterating a short line segment along the unstable direction of the period 2 orbit at (θ, ϕ). The structure is similar to the figures for the other billiard systems with pruning; the stable and the unstable manifolds have tent-like turning points instead of homoclinic tangencies, similar to the Lozi map, figure 5.20. We will return to this below in order to describe the pruning. In figure 7.3 we sketch how a line is folded in order to yield the tent like structure in figure 6.12.

6.5.2 Symbolic dynamics

As for the disk billiards, it is necessary to have different symbols for the different parts of the wall. However, as noticed by Biham and Kvale is also necessary to have some distinction between a clockwise and an anticlockwise bounce in the semi-circular part. Otherwise would we not be able to distinguish between two orbits such as the two drawn in figures 6.13 a) and b). The first guess is to give one symbol to each straight line and for a bounce in the semi-circle to distinguish between if it is the right or the left semi-circle and if it is a clockwise or anticlockwise bounce with respect to the center of the semi-circle. This gives a six letter alphabet which we believe is covering such that any admissible orbit in the billiard has a unique symbol string as its symbolic description, and no other orbits are described by the same symbol string but there will be symbol strings which do not correspond to any orbit. We show below that this alphabet has the unpleasant feature that with it there seems to be no way to find a finite Markov graph of the stadium, even in the $a \to \infty$ limit. Figure 6.14 shows the definition of this alphabet $s_t^a \in \{0, 1, 2, 3, 4, 5\}$.:

$s_t^a = 0$ a bounce off the bottom line.

$s_t^a = 2$ a bounce off the upper line.

$s_t^a = 1$ a clockwise bounce off the left semi-circle.

$s_t^a = 4$ an anticlockwise bounce off the left semi-circle.

$s_t^a = 3$ an anticlockwise bounce off the right semi-circle.

$s_t^a = 5$ an clockwise bounce off the right semi-circle.

Orbits that go through the center of the semi-circle have to be treated specially, but for the moment we give these orbits both the symbol for a clockwise and an

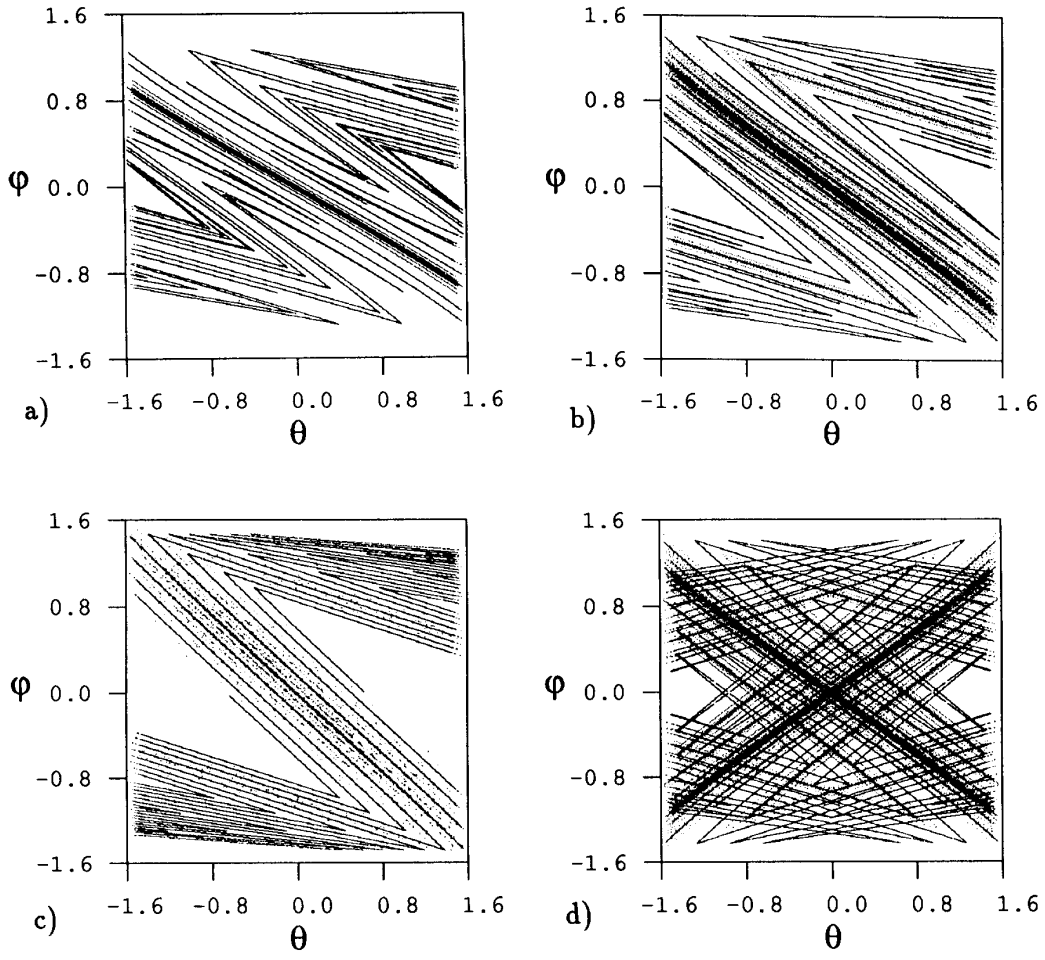

Figure 6.12: The unstable manifold of the periodic orbit at $(\theta, \phi) = (0, 0)$ in the stadium billiard with θ the position on the semi-circle and ϕ the outgoing angle for a) $a = 0.5$ b) $a = 1.0$ c) $a = 5.0$. d) Stable and unstable manifold for $a = 1.0$.

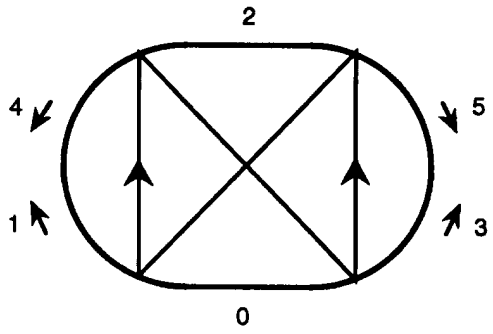

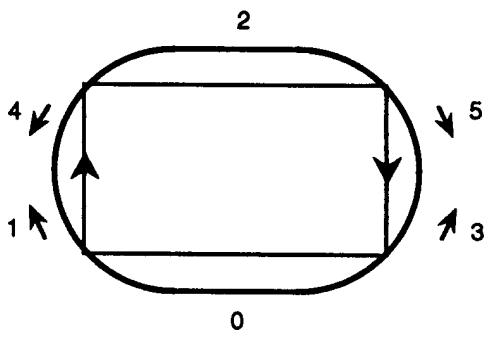

Figure 6.13: Two different period 4 orbits illustrating the necessity of distinguishing clockwise and anticlockwise bounces. a) $\overline{s_1^a s_2^a s_3^a s_4^a} = \overline{1133}$, b) $\overline{s_1^a s_2^a s_3^a s_4^a} = \overline{1155}$.

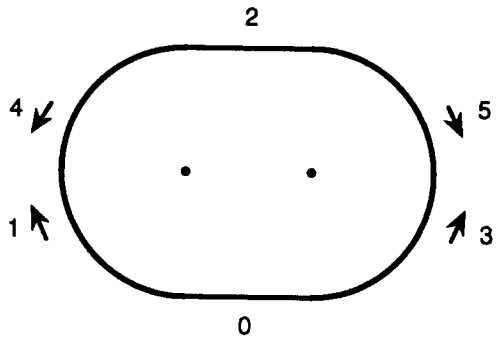

Figure 6.14: The symbols s_t^a in the stadium.

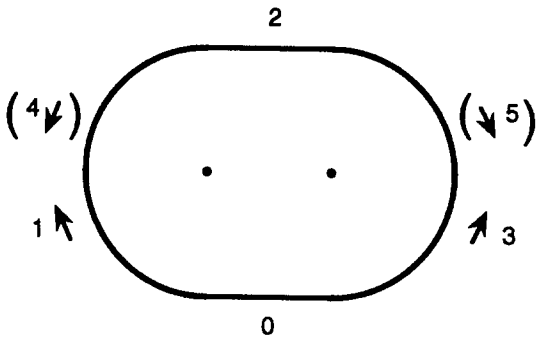

Figure 6.15: The Biham-Kvale symbols s_t^b.

anticlockwise bounce, and keep in mind that such orbits are double counted.

The alphabet introduced by Biham and Kvale [25] is a small modification of this alphabet which remove the degeneracy counting orbits through the center. They use a 6 letter alphabet $s_t^b \in \{0,1,2,3,4,5\}$ as above, but if an orbit bounces only once in a semi-circle then they denote it by the same symbol independent of whether it bounced clockwise or anticlockwise. They choose to let a single bounce that had symbol $s_t^a = 1$ still has the symbol $s_t^b = 1$ while a single bounce with $s_t^a = 4$ is renamed to $s_t^b = 1$. A single bounce that had symbol $s_t^a = 3$ still has the symbol $s_t^b = 3$, while a single bounce with $s_t^a = 5$ is renamed to $s_t^b = 3$. Figure 6.15 illustrates the alphabet s_t^b.

Instead of working with symbols denoting each bounce as above we introduce symbols which describe how a bounce changes the path. This reduces the number of symbols to 5. In this alphabet will some orbits with the same length and stability be described by the same symbol string. An important observation is that a single

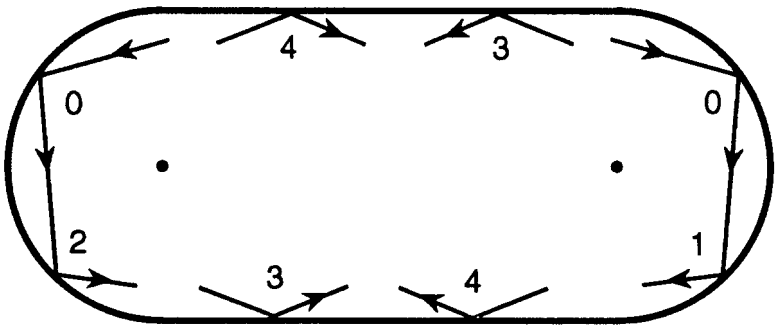

Figure 6.16: The symbols s_t^c in the stadium.

bounce should not distinguish between clockwise and anticlockwise. We define a new alphabet s_t^c as follows:

$s_t^c = 0$ if the bounce is the first bounce in a semi-circle,

$s_t^c = 1$ if the bounce is clockwise in a semi-circle and not the first bounce in the semi-circle,

$s_t^c = 2$ if the bounce is anticlockwise in a semi-circle and not the first bounce in the semi-circle,

$s_t^c = 3$ if the bounce is either in the bottom line in the direction to the right or if it is a bounce in the top line going to the left,

$s_t^c = 4$ if the bounce is either in the bottom line in the direction to the left or if it is a bounce in the top line going to the right.

These symbols are illustrated in figure 6.16.

To determine the well ordered symbols for the stadium we have to observe how the symbols change as we move a point in the phase space. The symbols s_t^a can be changed into well ordered symbols by observing the change in symbols in figure 6.17. The figure shows how the next symbol change under monotone increase of the outgoing angle, starting with one of the 6 symbols. From the figure 6.17 a) we find that starting at the bottom line with symbol $s_t^a = 0$ gives for $\theta \to -\pi/2$ symbol $s_{t+1}^a = 3$ because the next bounce is a clockwise bounce in the right semi-circle. When θ increases then at some point the particle goes through the center of the right semi-circle and the symbol changes to $s_{t+1}^a = 5$. The value where it changes depends on the position and on the parameter. For even larger values of θ the particle hits the top straight line and then the next symbol is $s_{t+1}^a = 2$. For some value $\theta > 0$ the particle starts to hit the left semi-circle bouncing clockwise giving $s_{t+1}^a = 4$. Finally for some larger value of θ the particle moves through the center of the left semi-circle and for angles larger than this up to $\pi/2$ the

$s^a_{t-1}s^a_t$	v^a_t
03	0
05	1
02	2
04	3
01	4

$s^a_{t-1}s^a_t$	v^a_t
10	0
13	1
15	2
12	3
11	4

$s^a_{t-1}s^a_t$	v^a_t
24	0
21	1
20	2
23	3
25	4

$s^a_{t-1}s^a_t$	v^a_t
33	0
32	1
34	2
31	3
30	4

$s^a_{t-1}s^a_t$	v^a_t
44	0
40	1
43	2
45	3
42	4

$s^a_{t-1}s^a_t$	v^a_t
52	0
54	1
51	2
50	3
55	4

Table 6.1: Construction of the well ordered alphabet in the stadium billiard from the symbols s^a_t. The well ordered symbols w^a_t are constructed by choosing $w^a_t = v^a_t$ when the number of 0's and 2's (bouncing in a straight lines) in the symbol string $s^b_0 \dots s^b_{t-1}$ is *odd* and choosing $w^a_t = 4 - v^a_t$ when the number is *even*.

next symbol is $s^a_{t+1} = 1$. The ordering of the two symbols combination with the first symbol 0 is then: $\{03, 05, 02, 04, 01\}$ and we rename these combinations to be respectively $v^a = \{0, 1, 2, 3, 4\}$. The definition of the symbol v^a_t for the other two symbol combinations is given in table 6.1. Symbols v^a_t are analogue to symbols s_t for the Smale horseshoes and the symbols v_t of the disk billiards. These symbols are correctly ordered for one bounce but not globally.

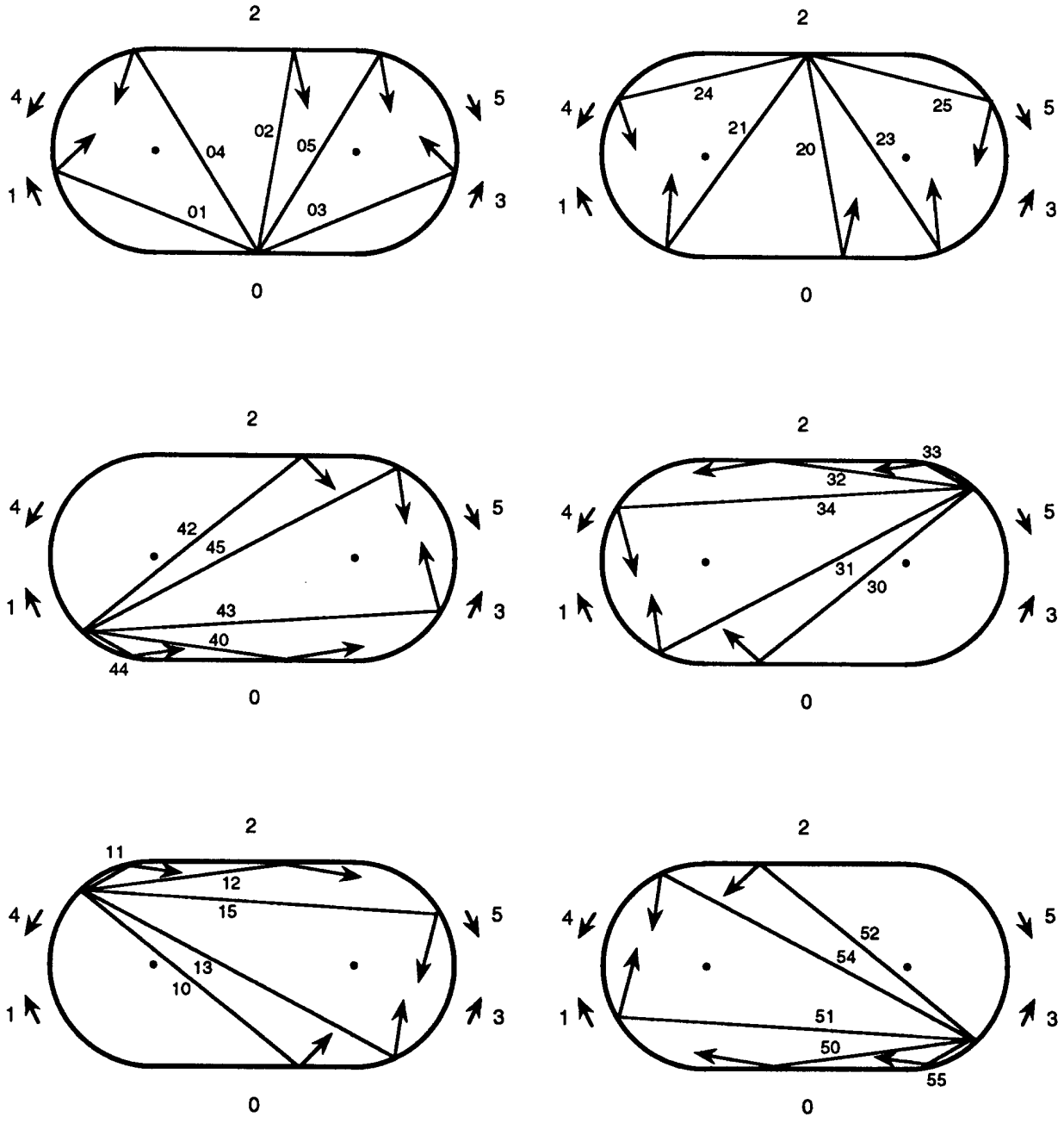

Figure 6.17: Construction of the well ordered symbols from symbols s^a, see table 6.1.

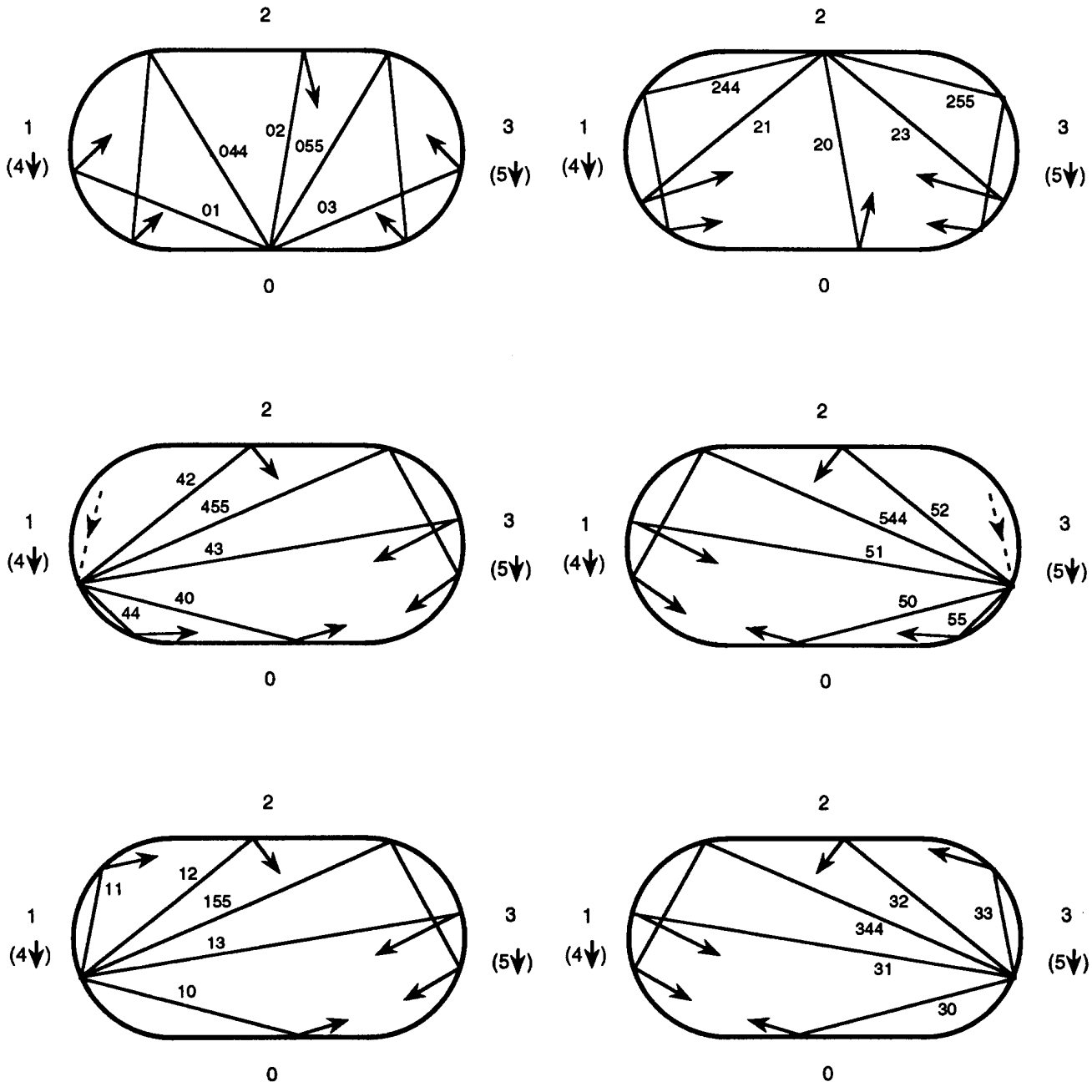

Figure 6.18: Construction of the well ordered symbols from symbols s^b, see table 6.2.

$s_t^b s_{t+1}^b (s_{t+2}^b)$	v_{t+1}^b
03	0
055	1
02	2
044	3
01	4

$s_t^b s_{t+1}^b (s_{t+2}^b)$	v_{t+1}^b
44	0
40	1
43	2
455	3
42	4

$s_t^b s_{t+1}^b (s_{t+2}^b)$	v_{t+1}^b
10	0
13	1
155	2
12	3
11	4

$s_t^b s_{t+1}^b (s_{t+2}^b)$	v_{t+1}^b
244	0
21	1
20	2
23	3
255	4

$s_t^b s_{t+1}^b (s_{t+2}^b)$	v_{t+1}^b
52	0
544	1
51	2
50	3
55	4

$s_t^b s_{t+1}^b (s_{t+2}^b)$	v_{t+1}^b
33	0
32	1
344	2
31	3
30	4

Table 6.2: Construction of the well ordered alphabet in the stadium billiard from symbols s_t^b. The well ordered symbols w_t^b are constructed by choosing $w_t^b = v_t^b$ when the number of 0's and 2's (bounces off straight lines) in the symbol string $s_0^b \ldots s_{t-1}^b$ is odd and choosing $w_t^b = 4 - v_t^b$ when the number is $even$.

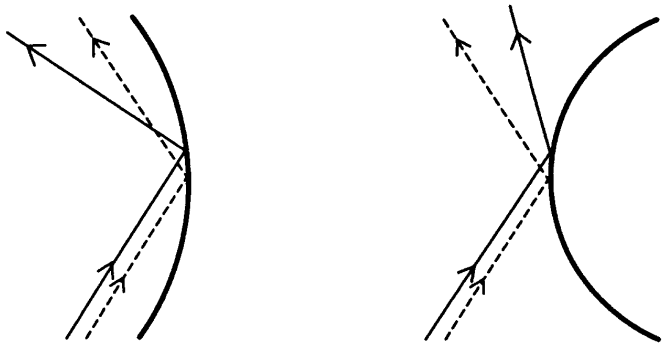

Figure 6.19: Orientation change for a bounce off; a) a convex, b) a concave wall.

In order to construct well ordered symbols we have to know how the manifolds flip at a bounce. A bounce in a focusing (convex) wall does not change orientation; figure 6.19 a) illustrates that two close orbits have the same relative orientation after a bounce as before the bounce. A bounce off a straight line reverses the directions in the same way as a dispersing wall in figure 6.19 b), so we have to count the number of straight wall bounces. If p_t is the number of symbols 0 and 2 in the sequence $s_0^a s_1^a s_2^a \dots s_{t-1}^a$, the well ordered symbols are given by

$$w_t^a = \begin{cases} v_t^a & \text{if } p_t \text{ odd} \\ 4 - v_t^a & \text{if } p_t \text{ even} \end{cases} \tag{6.28}$$

The symbolic value γ^a is now given as a real number in base 5

$$\gamma^a = 0.w_1^a w_2^a w_3^a \dots = \sum_{t=1}^{\infty} \frac{w_t^a}{5^t} \tag{6.29}$$

The simplest way to find the well ordered symbols of the past is to change the symbolic description of the past into a string of future symbols. Reversing the time for an orbit change all clockwise bounces into anticlockwise bounces and all anticlockwise bounces into clockwise bounces. This implies that symbol 1 becomes 4, 4 becomes 1, 3 becomes 5 and 5 becomes 3. Then the symbols $w_t^{a\prime}$ obtained from table 6.1 and algorithm (6.28) gives the well ordered symbols of the past. The symbolic value of the past is then

$$\delta^a = 0.w_1^{a\prime} w_2^{a\prime} w_3^{a\prime} \dots = \sum_{t=1}^{\infty} \frac{w_t^{a\prime}}{5^t} \tag{6.30}$$

The Biham-Kvale symbols v_t^b yield well ordered symbols and symbolic values γ^b and δ^b in the same way.

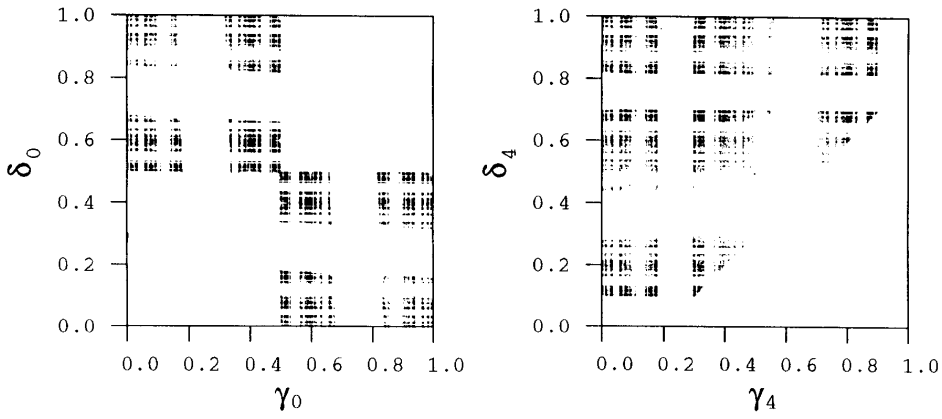

Figure 6.20: A chaotic trajectory in the symbol plane (γ^a, δ^a) for $a = 5.0$. Symbolic values for bouncing off a) the straight line, b) the semi-circle.

6.5.3 Symbolic dynamics in the limit $a \to \infty$

The description of the orbits in the stadium in the limit $a \to \infty$ depends on the choice of symbolic dynamics. We first show how the alphabet s_t^a gives a very complicated description and then how the other alphabets simplify the description.

The pruning depends on the parameter a monotonically, with the number of admissible orbits orbits increasing with increasing a. In the limit $a \to \infty$ we have as many orbits as it is possible to have in the stadium billiard. The topological entropy is largest for $a \to \infty$ and decreases monotonically with a.

By iterating a long chaotic orbit and plotting the symbolic values (γ^a, δ^a) for each bounce we obtain figure 6.20. In figure 6.20 a) the points (γ^a, δ^a) are plotted for the bounces with $s_0^a = 0$; we denote this symbol plane (γ_0^a, δ_0^a). In figure 6.20 b) the points (γ^a, δ^a) are plotted for the bounces with $s_0^a = 1$; we denote this symbol plane (γ_1^a, δ_1^a). The symbol plane for $s_0^a = 2$ is identical to (γ_0^a, δ_0^a), the symbol planes for $s_0^a = 3$ is identical to the plane (γ_1^a, δ_1^a) and the symbol planes (δ_4^a, γ_4^a) and (δ_5^a, γ_5^a) are identical to (γ_1^a, δ_1^a).

White regions in the plot of the symbol plane are forbidden regions corresponding to symbol strings that never appear in the dynamics. When we choose a large value of the parameter like $a = 5$ in figure 6.20, the visible forbidden regions are mostly the parameter independent $(a \to \infty)$ pruned regions.

In figure 6.20 a) we find that the two squares $\gamma_0^a > 1/2, \delta_0^a > 1/2$ and $\gamma_0^a < 1/2, \delta_0^a < 1/2$ are forbidden regions. The first region $\gamma_0^a > 1/2, \delta_0^a > 1/2$ translated back to the symbols s_t^a, contains all strings where a bounce in a straight line (symbol 0 or 2) has as its last symbol before a string of 0 and 2 symbols a bounce in the left

semi-circle (symbol 1 or 4). Also the first semi-circle symbol after this string of 0 and 2 symbols is a bounce in the left semi-circle (symbol 1 or 4). These are the forbidden strings 101, 1021, 10201,..., 104, 1024,.... The second square is the corresponding strings with bounces in the right semi-circle 303, 3023, 30203,..., 305, 3025,.... The limit of the regions are the lines $\gamma = 1/2$ and $\delta = 1/2$, which are orbits of form $1(02)^\infty 1$, etc. Even thought that there is no finite list of forbidden strings covering these forbidden regions, the rules are simple and can be implemented by a Markov graph.

In figure 6.20 b) there is a triangle shaped forbidden region below the line $\delta = \frac{1}{5} + \gamma$. One short string in this region is the string $\ldots 3 \cdot 13 \ldots$. This string is forbidden because the string $\ldots 3 \cdot 1$ imply a bounce off the left semi-circle at a point *below* the center of the left semi-circle. If the particle bounces off this left semi-circle clockwise (symbol 1) and immediately hits the right semi-circle, this has to be at a point *above* the center of the right semi-circle, and since the orbit was above both centers of the two semi-circles this is a bounce 5 and cannot be turned into a symbol 3 by changing starting position and angle. The limit of this region $\delta = \frac{1}{5} + \gamma$ translated back to the s_t^a symbols imply that there is a string

$$\ldots s_{-n} \ldots s_{-2} s_{-1} s_0 s_1 s_2 \ldots s_n \ldots$$

and for all these symbols we have $s_{-n} = 0$ if $s_n = 0$, $s_{-n} = 2$ if $s_n = 2$, $s_{-n} = 4$ if $s_n = 1$, $s_{-n} = 1$ if $s_n = 4$, $s_{-n} = 5$ if $s_n = 3$ and $s_{-n} = 3$ if $s_n = 5$ such that s_{-n} is the time reversed of s_n. This is the string describing an orbit going through the center of the semi-circle at the bounce $t = 0$.

To understand why this is the limit, draw an orbit through the center of a semi-circle as in figure 6.21. For example the orbit is given either by the symbol string $\ldots 1502113442034 \ldots$ or by the string $\ldots 1502115442034 \ldots$since the bounce is normal to the disk, there are two possible ways to write this string in the s_t^a alphabet. Assume now that we change the orbit slightly such that the bounce that used to be normal becomes an anticlockwise bounce. The first symbol string with $s_0^a = 3$ is the correct symbolic description of this orbit. If we perturb the orbit more such that the symbol string $\ldots 1502113$ still describe the first part of the orbit the last part of the symbol string can only change the following way. The symbol $s_1 = 4$ can only change to 2 or 3 and not to 1 or 0. If $s_1 = 4$ then the symbol $s_2 = 4$ cannot change. If $s_1 s_2 = 44$ then $s_3 = 2$ can change to 5, 3, 0 or 4. If $s_1 s_2 s_3 = 442$ then $s_4 = 0$ can change to 3 and 5. If $s_1 s_2 s_3 s_4 = 4420$ then $s_5 = 3$ cannot change to any other symbol. If $s_1 s_2 s_3 s_4 s_5 = 44203$ then $s_6 = 4$ can only change to 2 or 3 and not change to symbol 1 or 0. These rules for all t exactly define the forbidden triangle $\delta < 1/5 + \gamma$.

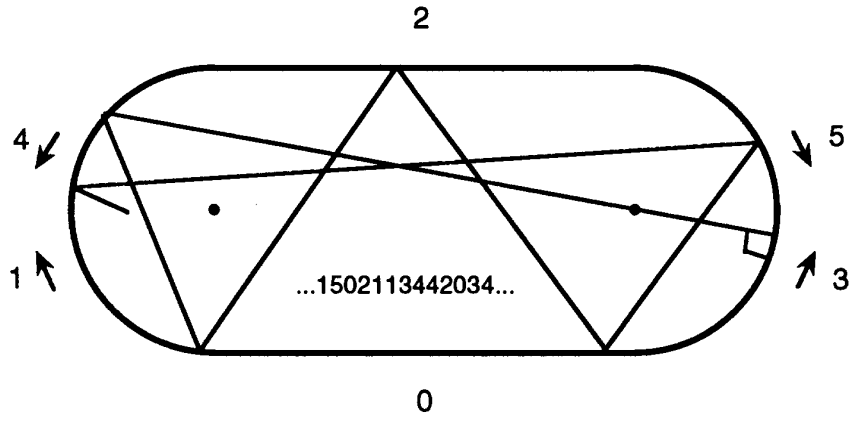

Figure 6.21: An orbit in the stadium going through one center of a semi-circle.

It seems to be extremely difficult to construct a Markov graph from these "triangle" rules. The symbolic string contains an infinite memory in a complicated way, and we have not been able to construct a finite Markov graph.

The simplest way to get rid of the triangle region is by not distinguishing between a right and a left bounce if there is only one simple bounce in the semi-circle as in the Biham and Kvale [25] alphabet s_t^b. This removes both the forbidden orbits of the triangle, and the double counting of the orbits bouncing normal to the semi-circle. We plot a long chaotic orbit in the symbol plane (γ^b, δ^b) for $a = 5$ in figure 6.22. In figure 6.22 a) the orbit is plotted in the symbol plane for bouncing off a straight line, with $s_0 = 0$, and in figure 6.22 b) for bouncing off the semi-circle with $s_0 = 4$. In (γ_0^b, δ_0^b) the same two squares are pruned as in (γ_0^a, δ_0^a). However in the (γ_4^b, δ_4^b) plane there is no triangular forbidden region as in the (γ^a, δ^a) plane. The largest forbidden regions are the rectangles $\gamma_4^b > 9/10$, $\delta_4^b < 1/10$, $2/10 < \gamma_4^b < 3/10$ and $7/10 < \delta_4^b < 8/10$. These are simple shifts of the squares in (γ_0^a, δ_0^a).

Biham and Kvale conjectured the forbidden orbits in the limit $a \to \infty$. Their forbidden orbits agrees with our forbidden square regions and in addition that the fixed points $\overline{1}$, $\overline{3}$, $\overline{4}$ and $\overline{5}$ do not exist. These fixed points are orbits bouncing infinitely many times in one semi-circle and these does not exist, while orbits bouncing any number of times in one semi-circle and then bounces somewhere else exist and are called "whispering gallery" orbits.

By using symbols s_t^b we can now construct a Markov diagram in the s_t^b symbols which gives all legal symbol strings. The only role that cannot be implemented is the forbidden fixed points $\overline{1}$, $\overline{3}$, $\overline{4}$ and $\overline{5}$, because only the fixed points are forbidden while any number of repetitions of the symbols are legal. We will discuss how this are implemented for the zeta-function in chapter 11. This graph is drawn in figure

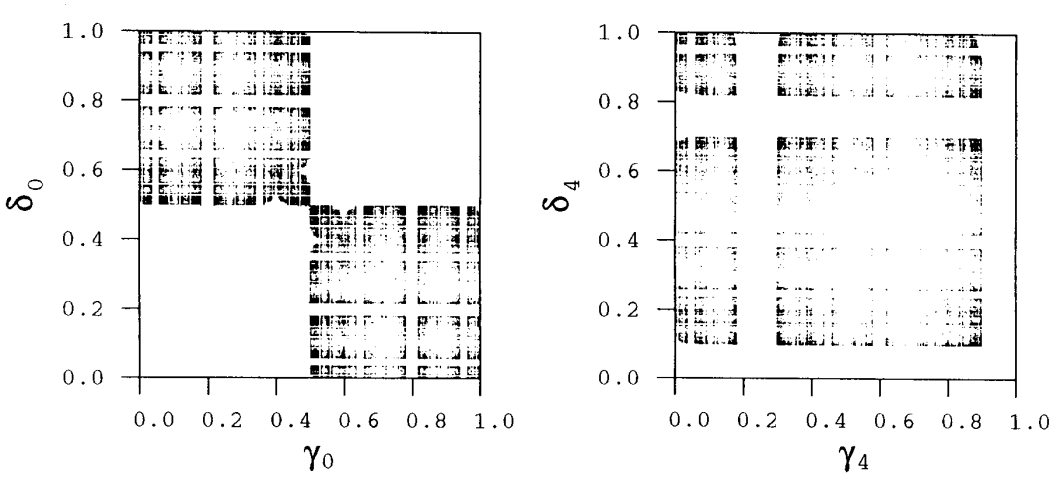

Figure 6.22: The points of a chaotic orbit in the symbol plane (γ^b, δ^b) for $a = 5.0$. Symbolic values for bouncing in a) the straight line $s_0 = 0$ b) the semi-circle with $s_0 = 4$.

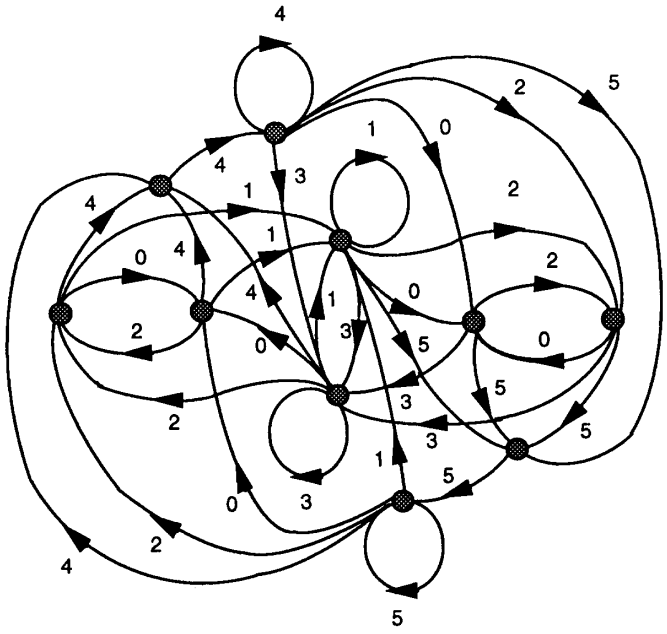

Figure 6.23: The Markov graph for the symbols s_t^b of the stadium.

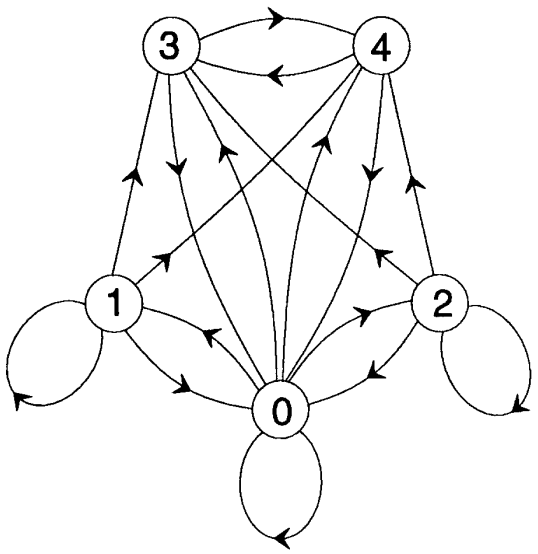

Figure 6.24: The Markov graph for stadium with alphabet s^c.

6.23 and it looks somewhat complicated. By using the method of counting loops and combinations of loops (section 1.3) we find the characteristic polynomial

$$p(z) = (1-z)^2(1+z)^2(1-z+3z^2+z^3)(1-3z-z^2-z^3) \tag{6.31}$$

All factors except the last one have to do with the symmetry of the graph [49] and the leading zero of the last factor gives the topological entropy:

$$z = -\frac{1}{3} - \frac{2^{\frac{8}{3}}}{3\left(13+3\sqrt{33}\right)^{\frac{1}{3}}} + \frac{2^{\frac{1}{3}}\left(13+3\sqrt{33}\right)^{\frac{1}{3}}}{3} = 0.2956\ldots \tag{6.32}$$

$$h = \ln z^{-1} = \ln 3.38298\ldots = 1.21875\ldots \tag{6.33}$$

We will show below that the graph can be simplified to figure 6.24 by using the alphabet s_t^c, and further to the graph in figure 6.25 using the alphabet s_t^d defined in table 6.3. The characteristic polynomial for the simple graph in figure 6.25 is

$$p(z) = 1-3z-z^2-z^3 \tag{6.34}$$

which is the last factor in (6.31) and the factor giving the topological entropy. That we have no other factors show that this alphabet s_t^d is in the fundamental domain and have no symmetries left.

The topological entropy is here not directly of physical interest for the dynamics because the "whispering gallery" orbits converge differently than the other orbits. It

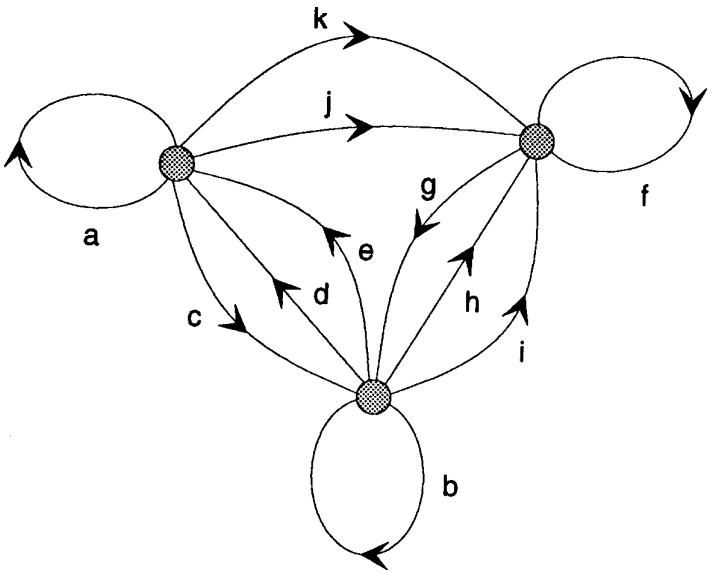

Figure 6.25: The reduced Markov graph for the stadium with alphabet s^d.

is however simple to calculate the topological entropy and it gives some information. In a complete horseshoe map the number of symbols is given as $\exp(h)$. This argument say that we here need 3.38 symbols in average to describe the possible orbits with these kind of orbits. In ref. [25] Biham and Kvale have calculated periodic orbits up to length 11 and they give the orbits which are left after applying geometrical pruning roles and from this table we find $h \approx \ln 3.1$ which is slightly less orbits than we expect from the diagrams. This may be due to the finite length of the orbits in Biham and Kvale's calculations.

The Markov graph, figure 6.24, describing the admissible orbits in the alphabet s_t^c are constructed by observing the following rules; The first bounce off a semi-circle,0, can be followed by a bounce off the other semi-circle, symbol 0, or by a second bounce off the same semi-circle either clockwise, symbol 1, or anticlockwise, symbol 2, or it can be followed by a bounce off one straight line with either symbol 3 or 4. These are the 5 arrows out from node 0 in figure 6.24. A second bounce in one semi-circle can be followed by a further bounce in the same semi-circle (with the same (anti-)clockwise direction) or by a bounce in the other semi-circle, symbol 0, or by a bounce in one of the two straight lines, symbol 3 or 4. This gives the 4 arrows out from the nodes 1 and 2 in figure 6.24. After a bounce in a straight line, symbol 3 or 4, a bounce in the other straight line has the opposite symbol as is clear from the inspection of figure 6.16. The other possible bounce after a straight line bounce is a first bounce in a semi circle, symbol 0. These two possibilities yields

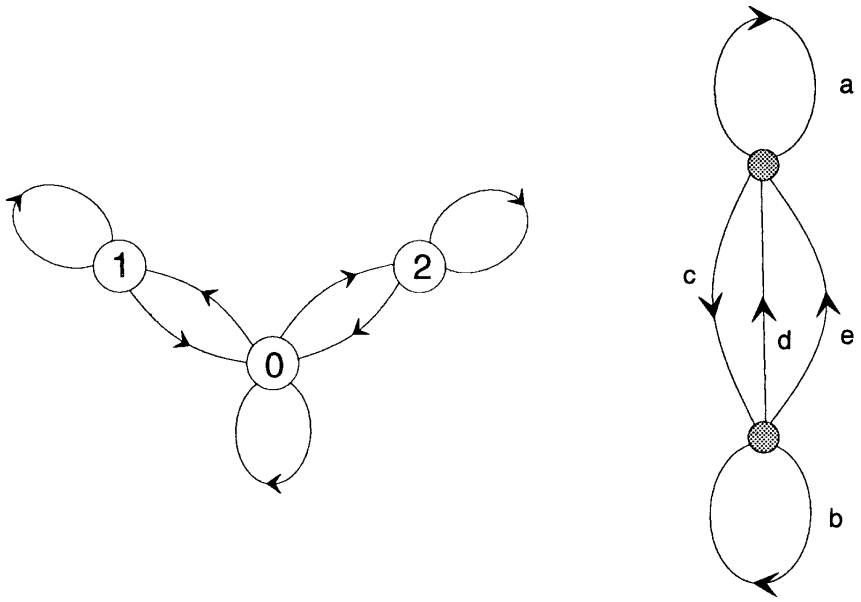

Figure 6.26: The reduced Markov graph for the simplified stadium scatterer. a) symbols s^c, b) symbols s^d.

the 2 arrows out from the nodes 3 and 4 in figure 6.24. Drawing the nodes and arrows gives the transition matrix in figure 6.24 with the characteristic polynomial

$$p(z) = (1-z)(1+z)(1-3z-z^2-z^3) \tag{6.35}$$

There is only half as many factors as in (6.31) since the alphabet s_t^c remove some of the symmetries.

To simplify this further and remove the symmetry in time and between clockwise and anticlockwise bounces we have to figure out which combinations of symbols that give the same segment of an orbit and which combinations of symbols that give essential different segments.

We define a fourth alphabet for the stadium in table 6.3, with symbols $s^d \in \{a, b, \ldots, k\}$. Symbols s^d are defined from two-symbol combinations of symbols s^c which in some cases depend on the symbolic string that preseeds the two-symbol configuration.

To understand why the dependence on the earlier symbols is necessary, look at the two symbol strings; s_t^c: $1(0)^n1$ and $2(0)^n2$. These two strings describe the same kind of segment of an orbit where the first string describes a clockwise orbit, and the second an anticlockwise orbit. A symbolic string $1(0)^n2$ describe a different kind of segment of an orbit which is symmetric to the segment described by the string $2(0)^n1$. Since the symbol 0 does not distinguish between clockwise and anticlockwise

s_t^d	$s_{t-1}^c s_t^c$	$\ldots s_{t-3}^c s_{t-2}^c s_{t-1}^c$
a	22	
	11	
b	00	
c	10	
	20	
d	01	$\ldots 1(0)^n$
	01	$\ldots 4(0)^n$
	02	$\ldots 2(0)^n$
	02	$\ldots 3(0)^n$
e	01	$\ldots 2(0)^n$
	01	$\ldots 3(0)^n$
	02	$\ldots 1(0)^n$
	02	$\ldots 4(0)^n$
f	34	
	43	
g	30	
	40	
h	03	$\ldots 2(0)^n$
	03	$\ldots 3(0)^n$
	04	$\ldots 1(0)^n$
	04	$\ldots 4(0)^n$
i	03	$\ldots 1(0)^n$
	03	$\ldots 4(0)^n$
	04	$\ldots 2(0)^n$
	04	$\ldots 3(0)^n$
j	23	
	14	
k	24	
	13	

Table 6.3: Definition for stadium symbols s^d from the symbols s^c.

bounces it is necessary to know the symbol preseeding the first 0 in a string of repeated 0's.

The Markov diagram in figure 6.25 with the s^d symbol is then constructed from labeling the arrows in the Markov diagram in figure 6.24, turning arrows into nodes and identify nodes with the same future. If we do not include the bounces in the straight lines $s^c = 3$, and $s^c = 4$ we obtain the diagrams in figure 6.26 a) and b). These diagrams are subsets of the full diagrams and describes the symbolic strings in the repellor consisting of only the two semicircles. These simpler diagrams can be constructed from inspecting the legal orbits in this repellor.

A difference between the s^d Markov graph and the preceding graphs is that in the preceding graphs the symbols can be associated either with the nodes or with the arrows between the nodes. In the s^d diagrams the symbols have to be associated with the arrows because there are two different arrows connecting the same two nodes.

The existence of the marginally stable periodic orbit bouncing between the two straight lines; s^a: $\overline{02}$ and the forbidden fixed points: s^a: $\overline{1}$, $\overline{3}$, $\overline{4}$, $\overline{5}$, suggests that we may introduce a new alphabet of the type applied in ref. [10] to study the Gauss map. We prefer however to construct the Markov graphs with includes all these special orbits, and when we find the expansion of the Zeta function from the graphs we sum up infinite families and avoid these orbits. This is further discussed in chapter 11.